Acta Biomaterialia 197 (2025) 202–215

Contents lists available at ScienceDirect

Acta Biomaterialia

journal homepage: www.elsevier.com/locate/actbio

Full length article

Osteogenic surgical sutures for tendon traction and fixation: A model of achilles tendon sleeve avulsion

Xiao Yu [a,1], Genbin Wu [b,1], Yangfan Ding [a], Panpan Shang [c], Pengfei Cai [d], Jie Cui [a], Jiahui Song [a], Jinglei Wu [a], Mohamed EL-Newehy [e], Meera Moydeen Abdulhameed [e], Xiumei Mo [a,c,*], Yinxian Yu [b,*], Binbin Sun [a,*]

[a] State Key Laboratory for Modification of Chemical Fibers and Polymer Materials, Shanghai Engineering Research Center of Nano-Biomaterials and Regenerative Medicine, College of Biological Science and Medical Engineering, Donghua University, 201620, Shanghai, PR China
[b] Department of Orthopedic Surgery, Shanghai General Hospital, Shanghai Jiao Tong University School of Medicine, Shanghai, 200240, PR China
[c] Institute of Biomaterials and Biomedicine, School of Food and Pharmacy, Shanghai Zhongqiao Vocational and Technical University, Shanghai 201514, PR China
[d] G.E.R.N. Research Center for Tissue Replacement, Regeneration & Neogenesis, Department of Orthopedics and Trauma Surgery, Faculty of Medicine, Medical Center-Albert-Ludwigs-University of Freiburg, 79085 Freiburg im Breisgau, Germany
[e] Department of Chemistry, College of Science, King Saud University, P.O. Box 2455, Riyadh 11451, Saudi Arabia

ARTICLE INFO

Keywords:
Tendon repair
Suture
Traction
Fixation
Osteogenesis

ABSTRACT

Currently, the repair of Achilles tendon sleeve avulsion is a challenge due to their limited research and particularly difficult treatment. In tendon repair surgery, the construction of bone tunnels is required for the suspensory fixation of ruptured tendon by sutures. However, due to the biologically inert of commonly used tendon sutures, postoperative fixation instability, bone tunnel enlargement, and even tendon reconstruction failure can easily occur under stressful conditions. In this study, core-spun nanoyarns containing β-tricalcium phosphate (β-TCP) were prepared by electrospinning to serve as surgical sutures for tendon traction and fixation. The suture of 6 core-spun nanoyarns spun again into one strand had stronger mechanical properties, which could effectively pull the tendon. The silk fibroin micron yarn of the suture core layer and the polycaprolactone/silk fibroin/β-TCP nanofibers of the shell layer demonstrated favorable biocompatibility, which facilitated cell adhesion and expression in the tendon and bone. In the repair surgery of the Achilles tendon sleeve avulsion in rabbits, compared with non-degradable and high mechanical properties commercial sutures, the β-TCP in the nanofibers of sutures could induce osteogenesis, thereby reducing the gap in the bone tunnel and preventing enlargement of the bone tunnel. In conclusion, the suture could weave the ruptured tendon, fix the tendon to the bone, promote the formation of new bone in the bone tunnel, avoid the instability of the existing commercial sutures to the bone tunnel, and ultimately improve the success rate of tendon repair surgery.

Statement of Significance: Nowadays, there is very limited research on the Achilles tendon sleeve avulsion model. This model presents challenges due to inadequate tendon tissue in the calcaneus for direct repair and insufficient bone tissue on the avulsed tendon for fixation. The incidence of this model is low, but treatment once it occurs is particularly difficult. In this study, we proposed to compound osteogenesis-promoting β-TCP materials onto nanoyarns to prepare surgical sutures that could weave the ruptured tendon, fix the tendon to the bone, induce osteogenesis, and reduce the gap in the bone tunnel, thus avoiding the instability of the existing commercial sutures in the bone tunnel, and ultimately improving the success rate of the surgery.

1. Introduction

Achilles tendon sleeve avulsion rupture is a rare injury [1]. When the Achilles tendon avulses from its calcaneal insertion distally as a continuous "sleeve," without a large bony element amenable to internal fixation, this is referred to as an Achilles sleeve avulsion [2]. This injury presents challenges due to inadequate tendon tissue in the calcaneus for direct repair and insufficient bone tissue on the avulsed tendon for

* Corresponding authors.
E-mail addresses: xmm@dhu.edu.cn (X. Mo), eastpool@sjtu.edu.cn (Y. Yu), binbin.sun@dhu.edu.cn (B. Sun).
[1] Xiao Yu and Genbin Wu contributed equally to this work.

https://doi.org/10.1016/j.actbio.2025.03.037
Received 3 November 2024; Received in revised form 5 March 2025; Accepted 18 March 2025
Available online 19 March 2025

fixation [3]. The low incidence of this injury has restricted clinical and basic research, but treatment, when necessary, is particularly difficult. During tendon repair surgery, it is necessary to establish a bone tunnel to reattach the ruptured Achilles tendon to the bone. However, the "windshield-wiper effect" and "bungee effect" occur frequently between the graft and the bone tunnel after surgery [4]. These phenomena may disrupt the biological healing process of the graft in the bone tunnel [4,5]. The local or cross-sectional area of the bone tunnel may widen in the first 12 weeks after surgery, and a large bone tunnel may hinder revision surgery and increase the demand for grafts in staged surgery [6,7]. Bone loss around the graft directly affects the firm bonding between the grafted tendon and the bone tunnel, resulting in a higher failure rate in repair [8]. Thus, an effective match between these soft grafts and the bone tunnel with high hardness is the key to the success of the repair surgery [9].

In order to provide a stable and relatively static contact between the tendon graft and the bone tunnel, many fixation methods have been developed, such as interference screw fixation, endobutton fixation, and cross-pin fixation systems [7,10]. The majority of tendon grafts are fixed with screws, which have been demonstrated to have a high success rate. However, the screw itself usually occupies a considerable space within the bone tunnel, which limits the contact between the graft and the sidewall of the bone tunnel, thereby limiting the integration of the graft with the surrounding bones and ultimately affecting the bonding strength [10]. Furthermore, it is important to consider that if the bone is insufficiently large or exhibits relative fragility, the insertion of screws may result in fracture [11]. In addition, the expense associated with screws is considerable [12]. Therefore, it is essential to accelerate the integration of graft and bone tunnel, avoid fracture, improve the repair success rate, and reduce the cost of tendon repair surgery. Douglas *et al.* [13] reported that the suture fixation of the graft could greatly improve the stability. Matthai *et al.* [14] used stainless steel wire as an anchor for the graft to the tibia and femur. It could be used even when the femoral tunnel was ruptured, and the problem of mismatch between the length of the tunnel and the size of the graft could be avoided by adjusting the position of the graft in the tunnel. However, this stainless steel wire was biologically inert. He *et al.* [15] used Magnesium-Zinc-Gadolinium (ZG21) wire as a surgical suture to tighten the tendon fabric and pull it into the bone tunnel. The results showed that ZG21 wire could facilitate enhanced new bone growth, increased fibrocartilage-like tissue formation, and augmented bond strength. However, the ZG21 wire's remaining volume after 14 days of degradation *in vivo* was only 28.2 ± 2.3% of the original volume. If the suture degrades too quickly, it is difficult to ensure its usefulness in models that require long-term repair with mechanical support. Therefore, the development of biocompatible, degradation-matched, mechanically supported sutures is crucial.

Electrospun nanoyarns can be precisely sized and have stable, high-strength mechanical properties, which are suitable for tendon repair [16–18]. One of the most important points is that the nanoyarns obtained by mixing the spinnable materials in different proportions have controllable degradation rates and mechanical properties, so they can be made on demand [19]. In addition, it can mimic the microenvironment of the extracellular matrix (ECM), thus facilitating cell attachment, proliferation, and differentiation [20,21]. Polycaprolactone (PCL) is a biodegradable polymer that has been approved by the US Food and Drug Administration for a variety of medical applications [22]. Silk fibroin (SF) is biocompatible, and SF-based scaffolds can promote the regeneration of soft tissues such as ligaments and tendons. In addition, it also can serve as filling materials for cartilage and bone repair [23]. β-tricalcium phosphate (β-TCP) is absorbable and can promote the proliferation and differentiation of mesenchymal stem cells, which can promote bone inward-growing through bone conduction [24,25]. Therefore, β-TCP has been widely used in bone tissue regeneration.

In this study, the core-spun nanoyarns containing β-TCP as surgical sutures were prepared by electrospinning. At first, the SF micron yarn is the reinforcing core of the core-spun nanoyarns, thereby imparting enhanced mechanical properties. Then, the nanofibers containing PCL, SF, and β-TCP were used to wrap the SF micron yarn to prepare the core-spun nanoyarns, and the nanofibers were biocompatible, which was beneficial for cell attachment in the bone tunnel. Finally, the core-spun nanoyarns were woven to prepare the tendon graft, which acted as a suture to wrap and tighten the ruptured tendon and then pulled into the bone tunnel to assist in fixation. In this process, the sutures could provide better initial fixation strength. The sutures then induced bone regeneration, which could reduce the gap between the sutures and the bone tunnel, and prevent the movement of the sutures in the bone tunnel. We have systematically evaluated the sutures at the *in vitro* cellular and *in vivo* animal levels.

2. Experiments and methods

2.1. Materials

Polycaprolactone (PCL, Mn 80,000, 440,744–250 G, Sigma-Aldrich), β-tricalcium phosphate (β-TCP, 99.5 %, BD114545–500 g, Bidepharm), silk fibroin micron yarn (SF micron yarn, Suzhou Huguang Mountain Velvet Development Co.), 1,1,1,3,3,3-hexafluoro-2-propanol (HFIP, Shanghai Jiu Ming Trading Firm), silk fibroin (SF). The following was the extraction method for SF: Firstly, Na_2CO_3 of 30 g was poured into deionized water of 6 L and boiled. Secondly, silkworm cocoons of 60 g were poured and boiled for 30 min. Repeat the above steps three times. Next, the boiled silkworm cocoons were torn and then dried in an oven. In addition, LiBr of 273 g was dissolved in deionized water to 350 mL. The torn silkworm cocoons were added to the LiBr solution and stirred until completely dissolved. Finally, the dissolved liquid was dialyzed for 5 days, then filtered and frozen dry to obtain SF.

Arthrex-FiberWire® suture (Art) was a common commercial suture constructed of a multi-strand, long chain ultra-high-molecular-weight polyethylene core with a braided jacket of polyester, which was provided by Shanghai General Hospital.

2.2. Electrospun sutures preparation

The mechanical properties of SF, PLA, PLGA, and polyethylene terephthalate (PET) micron yarns were compared from two aspects: Young's modulus and ultimate tensile strength (UTS) (Fig. 3A). Although the mechanical properties of SF, PLA, and PLGA micron yarns were not as strong as PET micron yarns, SF micron yarn had better mechanical properties among the three degradable micron yarns, so it was selected as the reinforcement core for electrospinning nanoyarn.

The electrospinning nanoyarn containing PCL, SF, β-TCP nanofiber membrane as the shell layer and SF micron yarn as the core layer was used as the suture for the ruptured tendon traction and fixation (Fig. 1). The preparation method was as follows: PCL (0.8 g), SF (1 g), and β-TCP (0 mg, 50 mg, 100 mg) were dissolved in HFIP (10 mL). The solution was stirred for 12 h until fully dissolved at room temperature. The solution was loaded into two syringes that were fixed at the positive and negative voltage of the electrospinning equipment. SF micron yarn was fixed to the receiving roller through the winding roller. Under high-speed rotation of the winder and high voltage, nanofibers of PCL/SF/β-TCP wrapped around SF micron yarn, which formed core-spun nanoyarns. Multiple core-spun nanoyarns could be combined and electrospinning again to obtain a thicker suture that could improve mechanical properties. For example, the 6 bundles of core-spun nanoyarns were combined and electrospinning again at their periphery to obtain a suture. The spinning parameters were: the voltage was 8 kV; the propulsion speed was 0.02 mL/min; the receiver speed was 10 rpm; and the winding roller speed was 400 rpm. The suture was cross-linked with 75 % alcohol vapor for 3 days. According to the type of nanofiber material and β-TCP mass to solution volume ratio, these electrospun sutures were named PS (PCL/SF), PS-T5 (PCL/SF/β-TCP- 5 mg/mL), and PS-T10 (PCL/SF/β-TCP- 10 mg/mL).

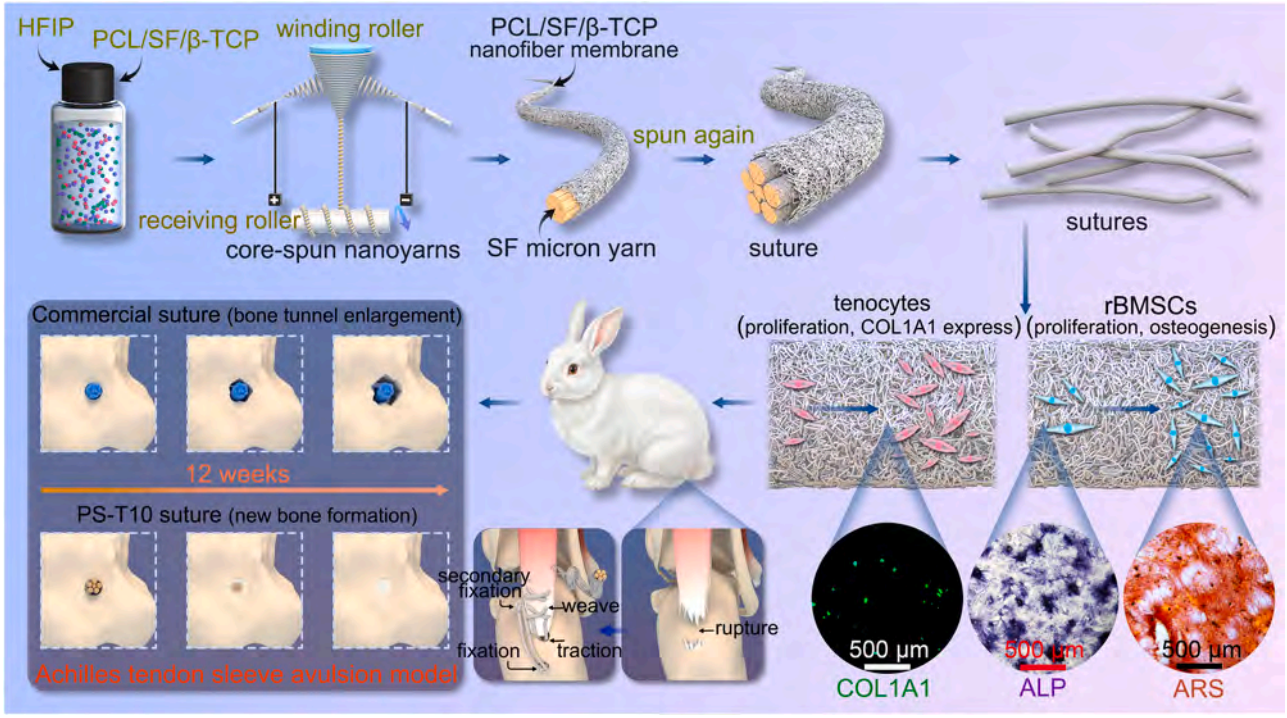

Fig. 1. Schematic illustration of the preparation and application of the suture. Firstly, the core-spun yarns were obtained by electrospinning, in which the reinforcing core was SF micron yarn and the nanofiber membrane was PCL/SF/β-TCP. Secondly, the 6 bundles of core-spun yarn were combined and spun again to obtain a thicker suture. Then, cells were seeded on the suture *in vitro*, which could promote rapid proliferation of tenocytes and expression of collagen I (COL1A1). In addition, it could promote the proliferation of rat bone marrow mesenchymal stem cells (rBMSCs) and the expression of alkaline phosphatase (ALP), alizarin red S (ARS), etc., which had the function of promoting osteogenesis. Finally, In the repair surgery of the Achilles tendon sleeve avulsion model in rabbits, the suture could weave the ruptured tendon, traction into the bone tunnel, and fixation the tendon to the bone. Compared with commercial suture, the PS-T10 suture could induce new bone formation, thereby reducing the gap in the bone tunnel and not causing bone tunnel enlargement, and ultimately improving the success rate of tendon repair surgery.

2.3. Electrospun sutures characterization

The sutures were characterized as follows: scanning electron microscopy (SEM), energy dispersive spectrometer (EDS), fourier transform infrared spectroscopy (FTIR), mechanical test, water contact angle test, thermogravimetric analysis (TGA), inductively coupled plasma emission spectrometer (ICP) detected Ca^{2+} release, and *in vitro* degradation test ($n = 3$). A detailed description of the related methods used can be found in the Supplementary material.

2.4. In vitro biocompatibility evaluation

MC3T3-E1 was obtained from the Cell Bank of the Chinese Academy of Sciences. rBMSCs and tenocytes were extracted from two-week-old SD rats according to the previous report [26,27]. The SD rats were purchased from Shanghai JieSiJie Laboratory Animal Co., Ltd. All cells were cultured in an incubator at 37 °C, 5 % CO_2, and the medium was changed every 2 days.

Different cells were used to evaluate the biocompatibility of the sutures (Art, PS, PS-T5, PS-T10). The experiments included cell seeding, cytotoxicity, migration, proliferation, fluorescence staining, and adhesion SEM ($n = 3$). A detailed description of the related methods was provided in the Supplementary material.

2.5. In vitro COL1A1 express ability of tenocytes

Tenocytes (2×10^4 pcs) were seeded, and cultured in the sutures extraction solution for 10 days. The tenocytes were stained with COL1A1, F-actin and DAPI ($n = 3$). A detailed description of the related methods was provided in the Supplementary material.

2.6. In vitro osteogenesis abilities of rBMSCs

The ALP and ARS activity, COL1A1, osteocalcin (OCN), osteopontin (OPN) and runt-related transcription factor 2 (RUNX2) immunofluorescence staining, and osteogenic gene expression that was evaluated by Quantitative Real-time PCR (qPCR) in rBMSCs to verify the osteogenesis abilities *in vitro* ($n = 3$). A detailed description of the related methods was provided in the Supplementary material.

2.7. Abilities of sutures to traction and fixation ruptured tendon in the bone tunnel

This study received ethical approval from Chedun Experimental Animal Breeding Farm Co., LTD., Songjiang, Shanghai.

The Art, PS, and PS-T10 sutures were used to validate the abilities of traction and fixation of the ruptured tendon in the calcaneus tunnel: adult rabbits were selected and each rabbit was injected with Zoletil 50 through the ear vein at a dose of 0.3 mL/kg. After the rabbit was anesthetized, the rabbit's left hind limb was shaved and sterilized. The skin was cut to expose the Achilles tendon and calcaneus. Then the Achilles tendon was separated from the calcaneus with a blade. The bone tunnel was drilled in the longitudinal direction of the calcaneus with a 1.5 mm Kirschner needle. Next, the sutures were equipped with 11 × 34 suture needles, and the ruptured Achilles tendon was weaved with two sutures, then the sutures were pulled into the bone tunnel. After the sutures were pulled out of the bone tunnel, they were folded in reverse, tied, and secured at the Achilles tendon. Therefore, the ruptured Achilles tendon was reattached to the calcaneus by sutures. Finally, the skin was sterilized with iodophor and sutured. Benzylpenicillin sodium was injected with 4×10^4 units/kg, three times a day for 3 days.

The repaired Achilles tendon and calcaneus samples after 4 and 12

weeks were treated with micro-computed tomography (micro-CT), hematoxylin-eosin staining (HE staining), Masson's trichrome staining (MT staining), immunofluorescence staining (IF staining), and mechanical tensile testing.

2.8. Statistical analysis

All data were expressed as mean ± standard deviation (SD) from three independent experiments with a minimum of three replicates for each condition. One-way analysis of variance (ANOVA) followed by Tukey's post hoc test was used to determine the statistical significance unless specified otherwise. The significant difference was considered at $*p < 0.05$ and $**p < 0.01$, $*** p < 0.001$.

3. Results

3.1. Characteristics of electrospun sutures

The suture was composed of 6 bundles of core-spun yarn, with a diameter of 0.86 ± 0.02 mm as observed under 240 X SEM. The presence of β-TCP between the nanofibers of PS-T5 and PS-T10 was discernible at 1000 X SEM, with the diameter of 620.16 ± 145.76 nm nanofibers (Fig. 2A). The presence of Ca and P in PS-T5 and PS-T10 suture that could be seen through EDS (Fig. 2B). From FTIR, the characteristic peaks of amide I and amide II of SF were observed at 1640 cm^{-1} and 1514 cm^{-1}, respectively. The carbonyl of PCL appeared at 1731 cm^{-1}, at the same time, the characteristic peaks of PCL at 733 cm^{-1} and β-TCP at 559 cm^{-1} could also be seen (Fig. 2C). Therefore, EDS and FTIR confirmed that SF, PCL, and β-TCP had been successfully spun into the sutures.

From the tensile mechanics results of the PS, PS-T5, and PS-T10, it can be seen that three sutures experienced a 12.60 ± 1.12 % strain at fracture, at which point the stress was 57.87 ± 3.04 MPa (Fig. 3B-D). The Young's modulus of the three sutures was 804.27 ± 56.01 MPa, and the maximum force was 28.23 ± 1.65 N (Fig. 3E and F). After 50 tensile cycles, the stress loss of the three sutures was 14.46 ± 1.65 % (Fig. 3G-I). It could be seen from the water contact angle test that three sutures were hydrophobic, and the hydrophobicity increased with the increase of β-TCP (Fig. 3J and K). The TGA curve of the sutures was consistent with SF micron yarn, and the mass loss mainly occurred at 200 °C - 800 °C, indicating that the sutures were thermally stable (Fig. 3L). The Ca^{2+} of β-TCP in PS-T5 could release 70.30 ± 0.06 μg/mL after 24 h, and PS-T10 could release 72.82 ± 0.25 μg/mL, which could sustain release for more than 30 days (Fig. 3M).

The degradation results of the SF micron yarn and three sutures after 1, 2, 4, and 8 weeks were as follows: with the increase of time, the SF micron yarn and the nanofibers on the surface of the sutures appeared to break, but the overall shape could be maintained intact (Fig. 4A & S1). After 8 weeks, SF micron yarn had a significant mass loss of 27.01 ± 7.21 %, and the mass loss of the PS, PS-T5, and PS-T10 was 13.56 ± 1.08 %, 14.73 ± 1.96 %, and 17.51 ± 3.79 %, respectively (Fig. 4B). The mass loss rate of PS-T5 and PS-T10 was faster than the PS, which was related to the release of β-TCP. The SF micron yarns were exposed to PBS, so the degradation rate was fast. Fortunately, in the sutures, the nanofiber on the surface played a protective role in the internal SF micron yarn, so the sutures degraded slowly, which contributed to prolonging the functionality of the sutures and could also be proved by

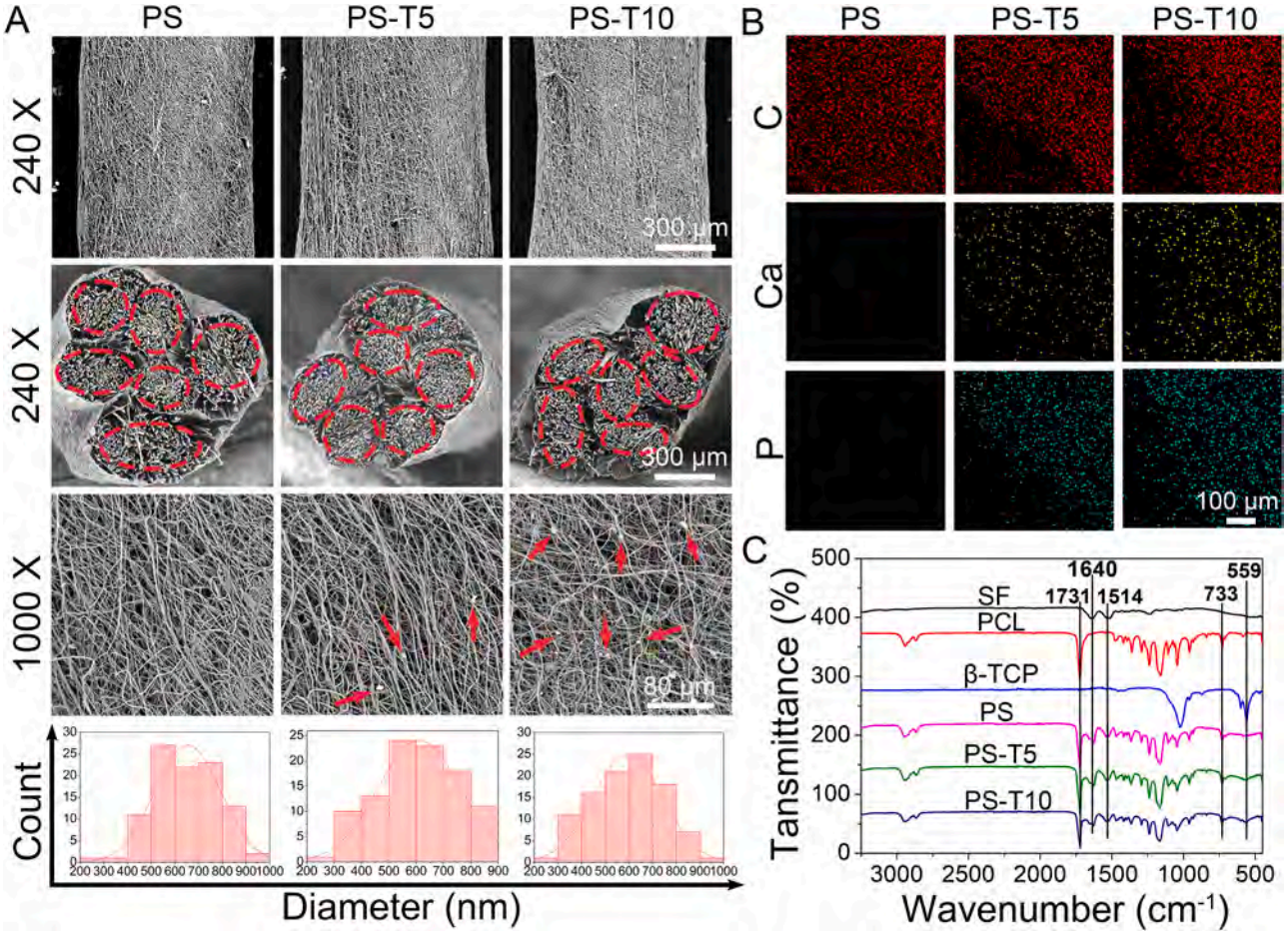

Fig. 2. (A) SEM images of the sutures at 240X and 1000X, and the nanofibers diameter statistics, scale bar = 300 μm, and scale bar = 80 μm. (B) EDS of the sutures, scale bar = 100 μm. (C) FTIR spectra of the SF, PCL, β-TCP, and sutures. Red arrows: β-TCP.

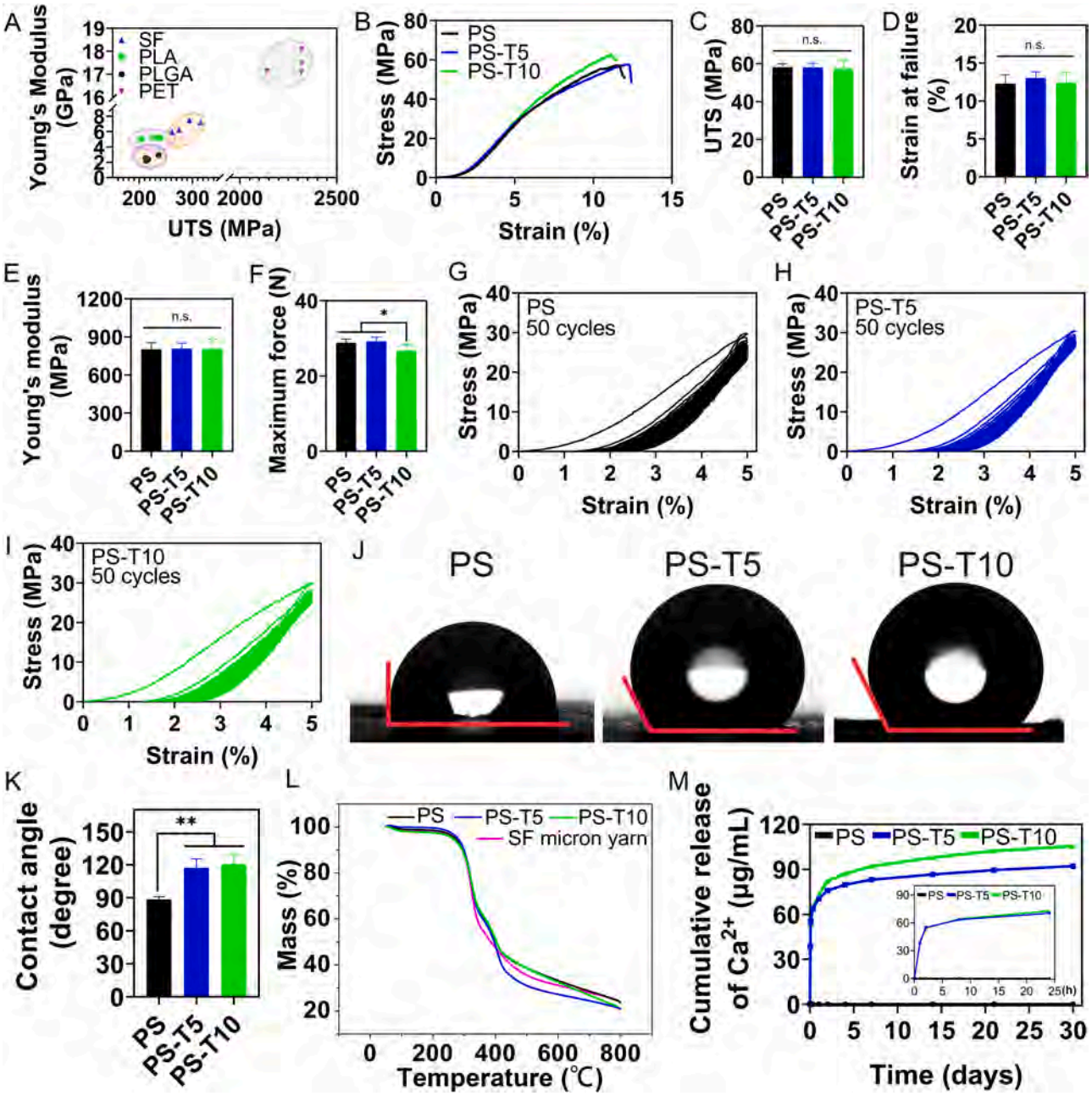

Fig. 3. (A) Mechanical comparison of SF, PLA, PLGA, and PET micron yarns. (B) The tensile stress-strain curves, (C) UTS, (D) strain at failure, (E) Young's modulus, and (F) maximum force of sutures, and (G) stress-strain curves for 50 cycles of PS, (H) stress-strain curves for 50 cycles of PS-T5, (I) stress-strain curves for 50 cycles of PS-T10. (J) The water contact angle of sutures and (K) contact angle statistics. (L) The TGA curves of SF micron yarn and sutures. (M) The Ca^{2+} cumulative release content of sutures. n.s.: no significance, * $p < 0.05$, ** $p < 0.01$.

the mechanical results after degradation. After 8 weeks, the UTS loss rate SF micron yarn was 93.57 ± 0.44 %, while the loss of PS, PS-T5, and PS-T10 was 56.22 ± 1.34 %, 41.13 ± 1.54 %, 28.55 ± 4.06 %, respectively (Fig. 4C and D). The Young's modulus loss rate of SF micron yarn was 96.52 ± 0.34 %, while the loss of PS, PS-T5, and PS-T10 was 58.23 ± 3.86 %, 50.19 ± 3.12 %, 56.20 ± 2.18 %, respectively (Fig. 4E and F). The maximum force loss rate of SF micron yarn was 82.01 ± 1.24 %, while the loss of PS, PS-T5, and PS-T10 was 56.87 ± 1.47 %, 48.86 ± 2.68 %, 32.57 ± 3.34 %, respectively (Fig. 4G and H). The results of the tests demonstrated that the SF micron yarn exhibited significant functional deterioration after 8 weeks, whereas the PS, PS-T5, and PS-T10 exhibited superior performance in all evaluated aspects. Compared to the human Achilles tendon [28], the sutures meet the mechanical requirements.

3.2. *Tenocytes biocompatibility and COL1A1 express*

To verify the difference between the sutures after electrospinning and commercial sutures (Art) in cell culture, the Art sutures were introduced as controls in cell experiments. From the CCK-8 results of tenocytes proliferation, it could be seen that the cell viability on the PS, PS-T5, and PS-T10 sutures was higher than that on the Art suture (Fig. 5A). The live/dead staining of tenocytes was consistent with CCK-8 results after 7 days, tenocytes spread more on the surface of the sutures of PS, PS-T5 and PS-T10 sutures, which were superior to the Art group (Fig. 5B). These results indicated that the sutures were biocompatibility and that PS, PS-T5 and PS-T10 were more conducive to tenocytes survival than Art.

The ability of tenocytes to form COL1A1 *in vitro* was verified by

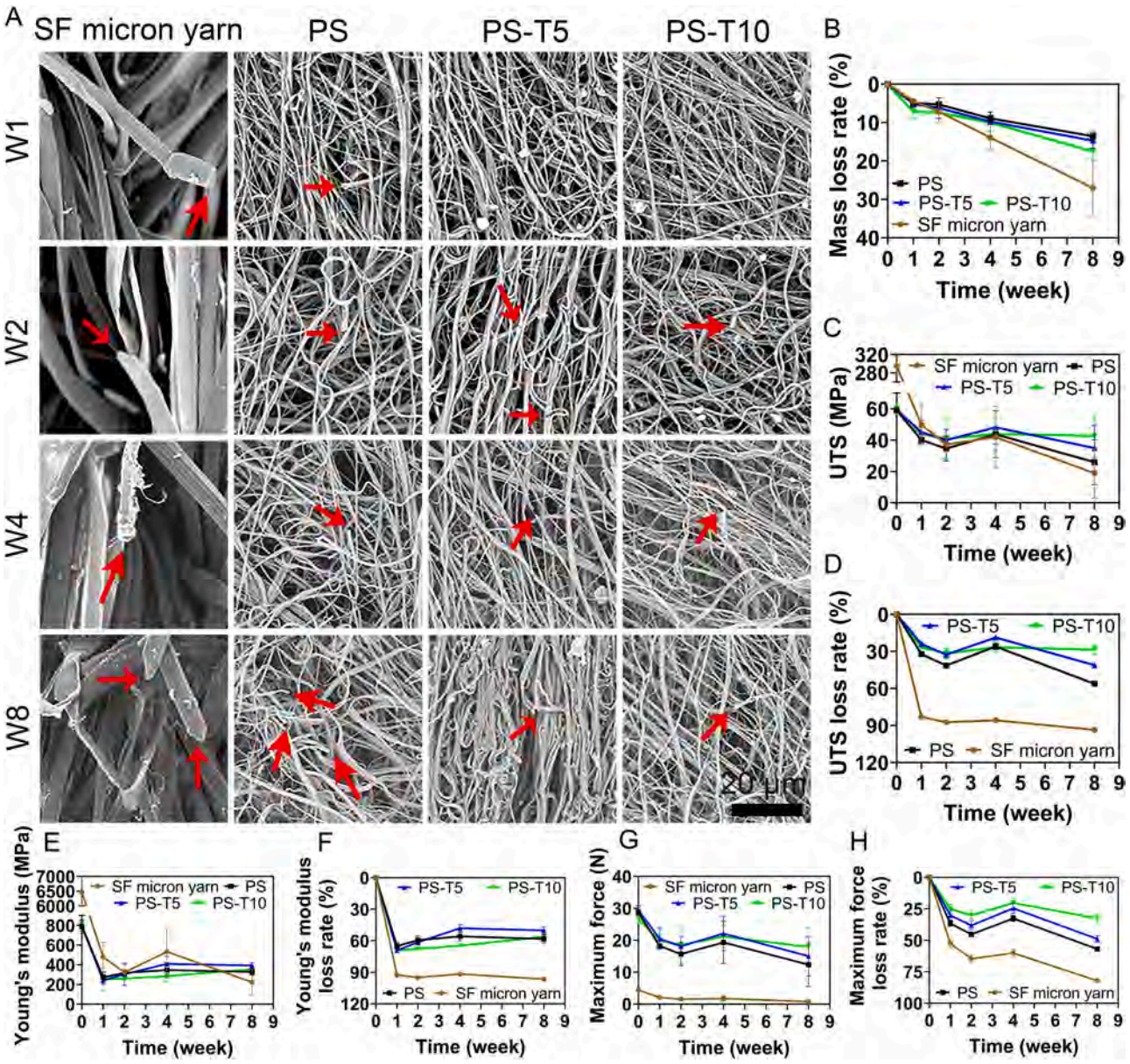

Fig. 4. (A) SEM, (B) mass loss rate, (C) UTS, (D) UTS loss rate, (E) Young's modulus, (F) Young's modulus loss rate, (G) maximum force and (H) maximum force loss rate of SF micron yarn and three sutures degradation after 1, 2, 4, and 8 weeks, scale bar = 20 μm. Red arrows: the SF micron yarn and nanofibers of three sutures broke.

DAPI/F-actin/COL1A1 staining when tenocytes were cultured for 10 days. The number of tenocytes in the PS-T5 and PS-T10 groups was significantly higher than that in the Art and PS groups (Fig. 5C and F). F-actin staining showed a large spread of tenocytes in the PS, PS-T5, and PS-T10 groups (Fig. 5D and F). Interestingly, the PS-T10 group has the highest COL1A1 expression ability (Fig. 5E and F).

3.3. MC3T3-E1 and rBMSCS biocompatibility

The cytotoxicity experiment of MC3T3-E1 showed that the cell viability of each group was higher than 75 %, indicating that the sutures were non-toxic (Fig. 6A). Transwell assay showed that PS-T5 and PS-T10 groups could promote the MC3T3-E1 migration (Fig. 6B and C). From the CCK-8 results, it could be seen that MC3T3-E1 and rBMSCs were all in a proliferative state (Fig. 6D). The results of live/dead staining of MC3T3-E1 were almost consistent with CCK-8, and the number of cells in the PS, PS-T5, and PS-T10 groups was more than that in the Art group (Fig. 6E). Both DAPI/F-actin staining and MC3T3-E1 morphology on sutures showed that MC3T3-E1 were able to spread over a large area, proving that the sutures were well biocompatible (Fig. 6F and G). rBMSCs showed proliferation and there was no obvious difference after 7 days among the PS, PS-T5, and PS-T10 suture, but all were significantly higher than the Art suture (Fig. 6H). The results of live/dead staining and SEM of rBMSCs after 7 days showed that the rBMSCs adhered to the Art suture in a dot or cluster shape, while the rBMSCs in the PS, PS-T5 and PS-T10 suture had better morphology and spread out in a spindle shape (Fig. 6I and J). These results suggested that the PS, PS-T5, and PS-T10 sutures were more suitable for the growth of rBMSCs than Art sutures.

3.4. In vitro osteogenesis abilities

The osteogenic ability of rBMSCs *in vitro* was evaluated by the expression of ALP, ARS, COL1A1, OPN, OCN, and RUNX2. For ALP activity between the groups after 7 days, there were no significant differences. With the increase of β-TCP content on the electrospun sutures,

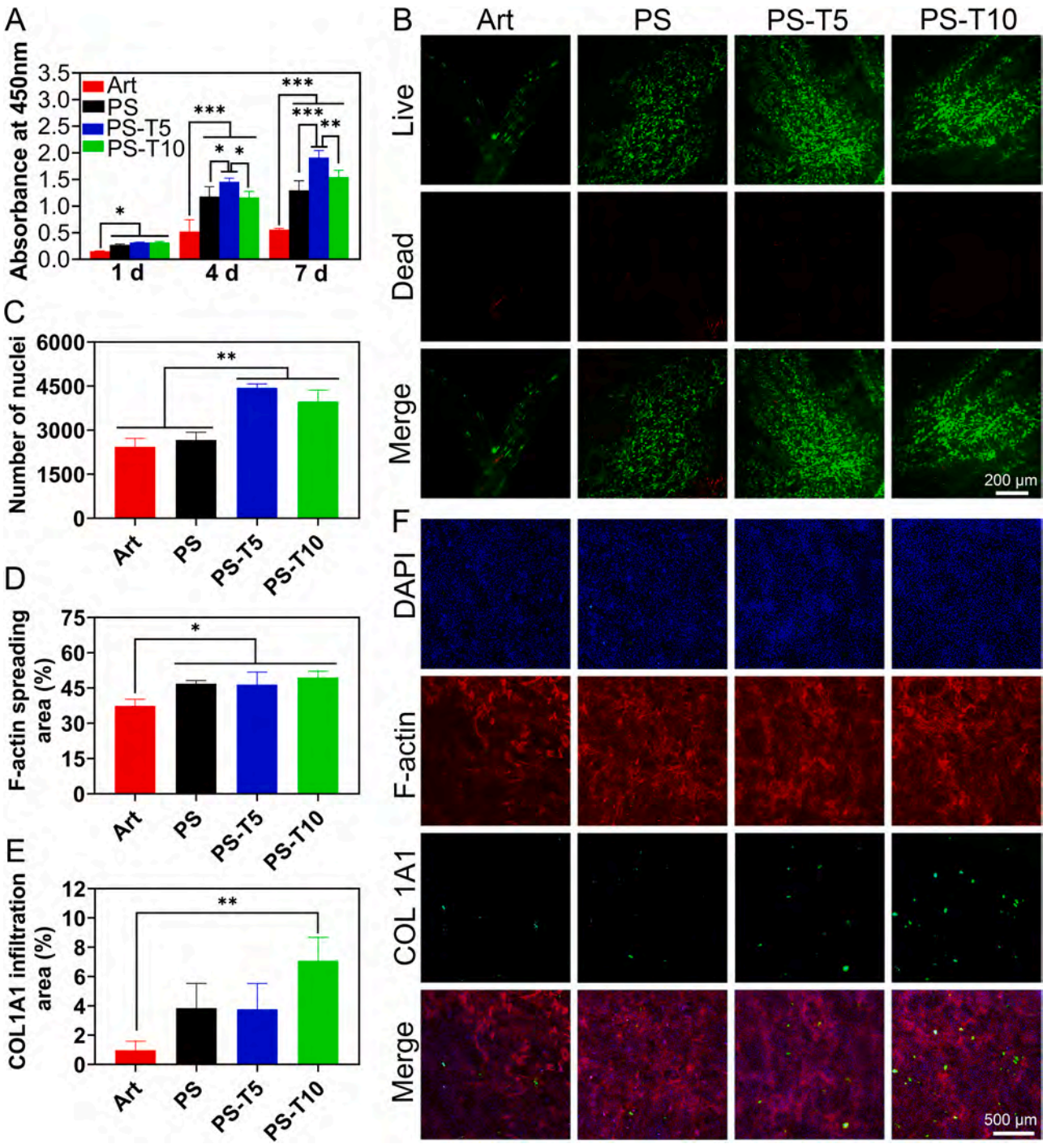

Fig. 5. (A) The proliferation of tenocytes on sutures was measured using the CCK-8 assay after 1,4, and 7 days. (B) Live/dead staining of tenocytes cultured on sutures after 7 days, scale bar = 200 μm. *In vitro* COL1A1 expression of tenocytes cultured in sutures extraction solution for 10 days: (C) the number of nuclei, (D) F-actin spreading area, (E) COL1A1 infiltration area statistics of tenocytes, and (F) tenocytes DAPI/F-actin/COL1A1 staining, scale bar = 500 μm. * $p < 0.05$, ** $p < 0.01$, *** $p < 0.001$.

ALP activity increased after 14 days, and both were significantly better than the Art group (Fig. 7A and C). The calcium deposition ability was detected by ARS, and it could be seen that the Art, PS-T5 and PS-T10 groups had stronger deposition capacity than the PS group after 14 days. Furthermore, the calcium deposition ability of the PS-T5 and PS-T10 groups was superior to the other two groups after 21 days, among which the PS-T10 group was the best (Fig. 7B and D).

The ability of rBMSCs to form COL1A1 *in vitro* was verified by DAPI/F-actin/COL1A1 staining when rBMSCs were cultured for 10 days. The number of rBMSCs in the PS-T10 group was significantly higher than that in the Art group (Fig. 7E and H). The rBMSCs of all the groups had a better spreading state, but the Art group had a slightly lower spreading area than the other groups, which was mainly due to its small number of rBMSCs (Fig. 7F and H). In COL1A1 staining, it could be found that the expression in PS-T5 and PS-T10 groups was significantly higher than that of the other two groups, indicating that the addition of β-TCP promoted COL1A1 expression (Fig. 7G and H). Meanwhile, other immunofluorescence staining of the rBMSCs revealed that the addition of β-TCP was more able to promote the expression of rBMSCs. Among them, PS-T10 expressed the highest level of OPN (Fig. 7I and L), and

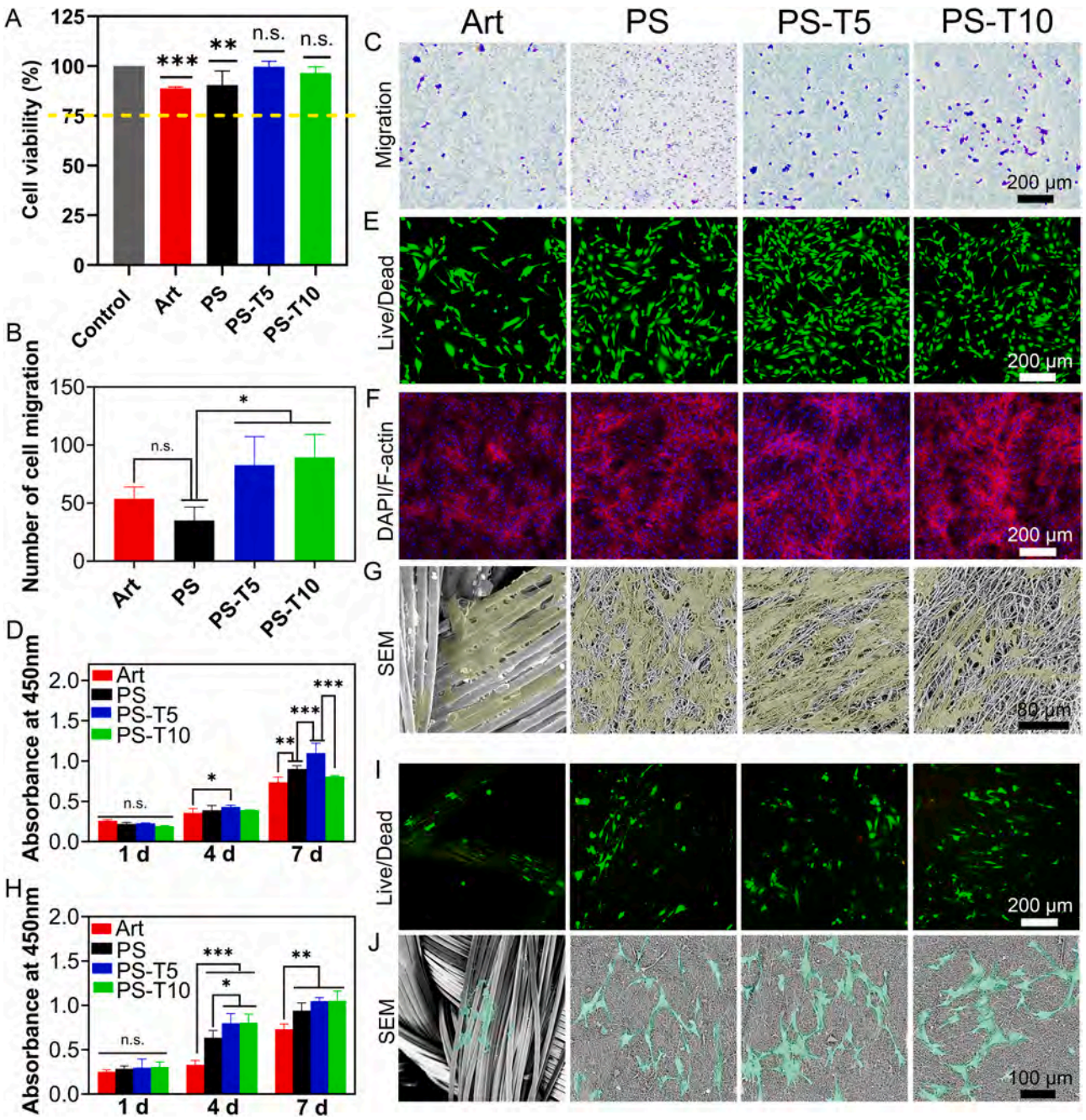

Fig. 6. *In vitro* biocompatibility evaluation. (A) Cell viability of MC3T3-E1, control: blank without sutures. (B) The number of cell migrations of MC3T3-E1, and (C) transwell migration staining, scale bar = 200 μm. (D) The proliferation of MC3T3-E1 on sutures was measured using the CCK-8 assay after 1,4, and 7 days. (E) Live/dead staining of MC3T3-E1 cultured in sutures extraction solution after 7 days, scale bar = 200 μm. (F) MC3T3-E1 DAPI/F-actin staining in sutures extraction solution after 10 days, scale bar = 200 μm. (G) MC3T3-E1 morphology on sutures after 7 days under SEM, scale bar = 80 μm. (H) The proliferation of rBMSCs on sutures was measured using the CCK-8 assay after 1,4, and 7 days. (I) rBMSCs live/dead staining on sutures after 7 days, scale bar = 200 μm, and (J) the rBMSCs morphology on sutures after 7 days under SEM, scale bar = 100 μm. n.s.: no significance, * $p < 0.05$, ** $p < 0.01$, *** $p < 0.001$.

expressed the highest level of OCN (Fig. 7J and M). The levels of RUNX2 expression in PS-T5 and PS-T10 were comparable, but both were higher than those in the Art and PS groups (Fig. 7K and N).

The gene expression associated with rBMSCs osteogenesis after 7 and 14 days was examined by qPCR. The detailed results are shown in Fig. 7O and P: the expression level of COL1A1 was the highest in the PS-T10 group after 7 days. After 14 days, on the one hand, there was no significant difference between the PS-T5 and PS-T10 groups, indicating that the COL1A1 expression ability was comparable. On the other hand, the COL1A1 expression levels in the PS-T5 and PS-T10 groups were higher than those of the other two groups, indicating that the addition of β-TCP could promote COL1A1 expression. These were similar to the results obtained with COL1A1 staining in Fig. 7G and H. The expression level of OPN was significantly different between the groups after 7 and 14 days. After 7 days, there was no significant difference in the expression level of OCN between the groups, but after 14 days, the expression level of PS-T10 was higher than the other groups. The expression level of RUNX2 showed no significant difference between the groups after 7 days, however, it was only highest in PS-T10 compared to PS after 14 days. These results indicated that PS-T10 had the best osteogenesis ability.

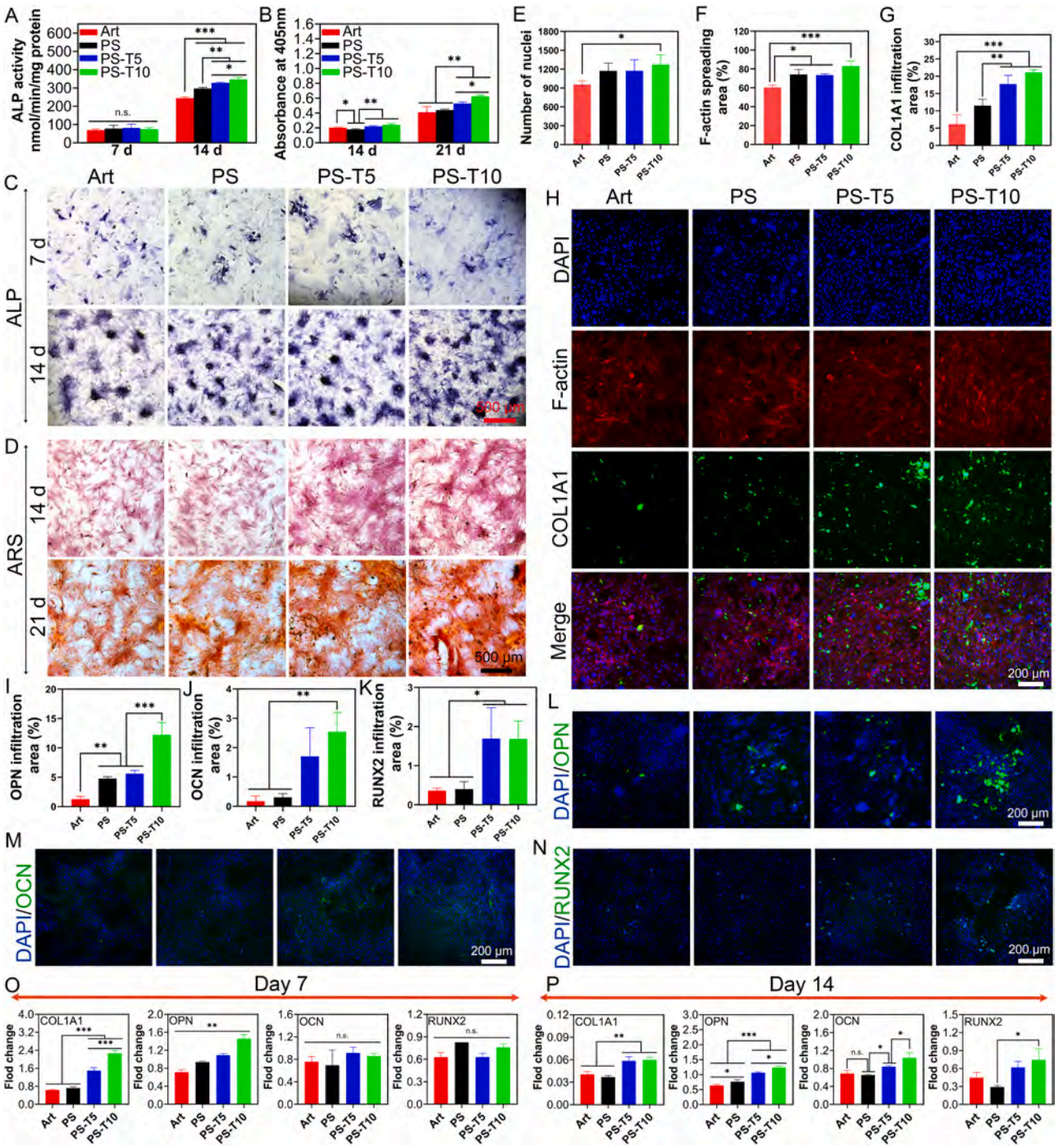

Fig. 7. *In vitro* osteogenesis abilities. (A) The measurement of ALP activity after 7 and 14 days. (B)The measurement of ARS activity after 14 and 21 days. (C) Microscopic images of ALP staining of rBMSCs after 7 and 14 days, scale bar = 500 μm. (D) Microscopic images of ARS staining of rBMSCs after 14 and 21 days, scale bar = 500 μm. *In vitro* COL1A1 expression of rBMSCs cultured for 10 days: (E) the number of nuclei, (F) F-actin spreading area, (G) COL1A1 infiltration area statistics, and (H) rBMSCs DAPI/F-actin/COL1A1 staining, scale bar = 200 μm. (I) OPN infiltration area statistics. (J) OCN infiltration area statistics. (K) RUNX2 infiltration area statistics. (L) DAPI/OPN staining, scale bar = 200 μm. (M) DAPI/OCN staining, scale bar = 200 μm. (N) DAPI/RUNX2 staining, scale bar = 200 μm. (O, P) The expression of osteogenic genes in rBMSCs after 7 and 14 days was analyzed by qPCR, including COL1A1, OPN, OCN, and RUNX2. n.s.: no significance, * $p < 0.05$, ** $p < 0.01$, *** $p < 0.001$.

3.5. Abilities of sutures to traction and fixation ruptured tendon in the bone tunnel

The ability of the suture to weave the tendon and fix the bone was verified by the Achilles tendon sleeve avulsion model (Fig. 8A). As can be seen from the macroscopic view, all three sutures could weave the ruptured Achilles tendon and then traction to the bone tunnel for fixation. After 4 weeks, the tendons in all three groups were able to attach to the calcaneus. At this point, the Art can be clearly seen exposed to the surface. The new tissue of the PS and PS-T10 groups was rougher, and the color of the sutures changed from white to yellow, which was caused by degradation. After 12 weeks, the coverage and roughness of the tissue between the tendon and the calcaneus were better in the three groups than in the 4 weeks. Because Art couldn't degrade, its

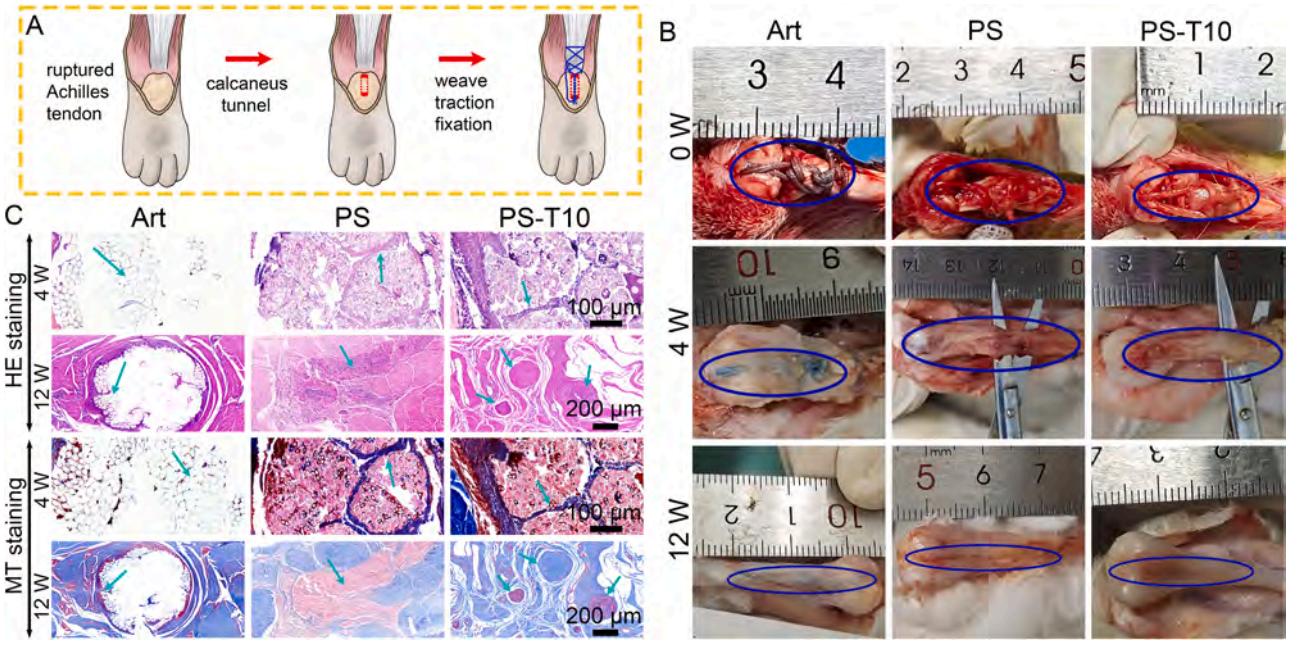

Fig. 8. The ability to repair tendon *in vivo*. (A) Repair model of Achilles tendon sleeve avulsion in rabbits. (B) Macroscopic view of Art, PS, PS-T10 sutures to weave the ruptured tendon and traction and fixation in the bone tunnel. (C) HE and MT staining of Art, PS, PS-T10 sutures weaving of the tendon after 4 and 12 weeks, scale bar = 100 μm, and scale bar = 200 μm. Green arrows: the position of the sutures.

appearance was visible, and its surface was covered by a thin layer of smooth tissue. The surface of tendon tissue in the PS group was still somewhat rough. Interestingly, the repair effect of the PS-T10 group was ideal with the degradation of the suture, in which smooth tissue replacement suture, and the connection between the tendon and calcaneus was not broken (Fig. 8B).

HE and MT staining of the tendon woven with sutures showed that the tendon tissue was difficult to grow into Art after 4 or 12 weeks, and the Art only occupied the position of the tendon tissue and could not be replaced by the tissue. After 4 weeks, the shape of the sutures in PS and PS-T10 groups was generally intact, in which some of the nanofibers on the surface of the sutures were replaced by tissue, and the internal SF micron yarns were not degraded and replaced. After 12 weeks, sutures were mostly replaced by tissues, but the collagen expression in the PS group was lower. The PS-T10 group showed an abundance of collagen where the suture was completely replaced by tissue, and collagen was also present in gap areas where the suture was partially replaced (Fig. 8C). The above showed that the PS-T10 suture had better biocompatibility and could be used for tendon weaving, which had a repairing effect on tendon defects.

After 12 weeks of micro-CT of the calcaneus, Art only occupied the position of the bone tunnel, and there was very little regenerated bone tissue. Unfortunately, in some of the Art groups, the bone tunnels were enlarged, making it impossible to calculate their BV/TV values (Fig. 9A and B). The bone tunnel in the PS group showed new bone but was not filled. PS-T10 bone tunnel had the most new bone, which provided the necessary conditions for the tendon to be firmly fixed to the bone tunnel (Fig. 9A and B).

At 4 weeks, HE and MT staining of the calcaneus showed that the tendon of the Art group was located in the bone tunnel with less cellular infiltration. Tissue ingrowth into the sutures was observed in both the PS and PS-T10 groups. The PS-T10 suture was covered with tissue and there was almost no gap was visible between the suture and the bone, but in PS was still a gap present between the suture and the bone. At this time, there was collagen expression in the periphery of the sutures in both the PS and PS-T10 groups, but very little collagen was expressed in their interior (Fig. 9C and D). After 12 weeks, consistent with the CT results, the Art suture caused the bone tunnel to expand and the original bone to disappear. In the PS group, the gap between the suture and bone was significantly reduced compared to 4 weeks, and sparse tissue was growing. The tissue between the suture and bone in the PS-T10 group was relatively dense, with almost no gaps visible. Moreover, PS-T10 after 12 weeks was significantly less inflammatory than PS and PS-T10 after 4 weeks, and there was collagen expression inside (Fig. 9C and D).

After 12 weeks, the IF staining showed that there was only a few cells grew into the bone tunnel in the Art group, and almost no expression of COL1A1 and OPN. Interestingly, the PS group had more cells attached to the sutures than PS-T10, but the expression of COL1A1 and OPN was highest at PS-T10 (Fig. 10A-D). Similarly, IF staining for RUNX2 and OCN was performed on the three groups and found to be most expressed in the PS-T10 group (Fig. 10E-G). These suggested that PS-T10 suture containing β-TCP had the greatest ability to promote cell osteoblastic differentiation. Mechanical tension was applied to the Achilles tendon-calcaneus, and when a small crack appeared in the tendon, the force-strain curve began to decrease (Fig. 10H and I). The PS group did not contain β-TCP, resulting in a slower bone formation rate and lower mechanical properties compared to the normal group (Fig. 10J). The commercial suture itself had strong mechanical properties, so it showed high strength in tissue stretching after 3 months, but this did not represent the strength of the tissue. Its non-degradation, non-integration, and ease of movement caused the tissue to show greater strain (Fig. 10K). The β-TCP released by the PS-T10 suture promoted the integration of the bone tissue, allowing its mechanics to improve. This also indicated that the tendons repaired with PS-T10 suture produced mechanical strength similar to commercial sutures (Fig. 10J and K).

4. Discussion

In tendon repair surgery, bone loss in the bone tunnel directly affects the strength of the tendon and bone tunnel bond, leading to repair failure [29,30]. The integration between the tendon and bone tunnel is crucial for the tendon repair [31]. Suture anchors containing β-TCP have been shown to have osteoconductive properties and are used clinically nowadays, but more than 90 % of suture anchors are still structurally visible after 2 years, further limiting bone growth of autologous bone at this site due to the slow rate of degradation [32]. Screw fixation has

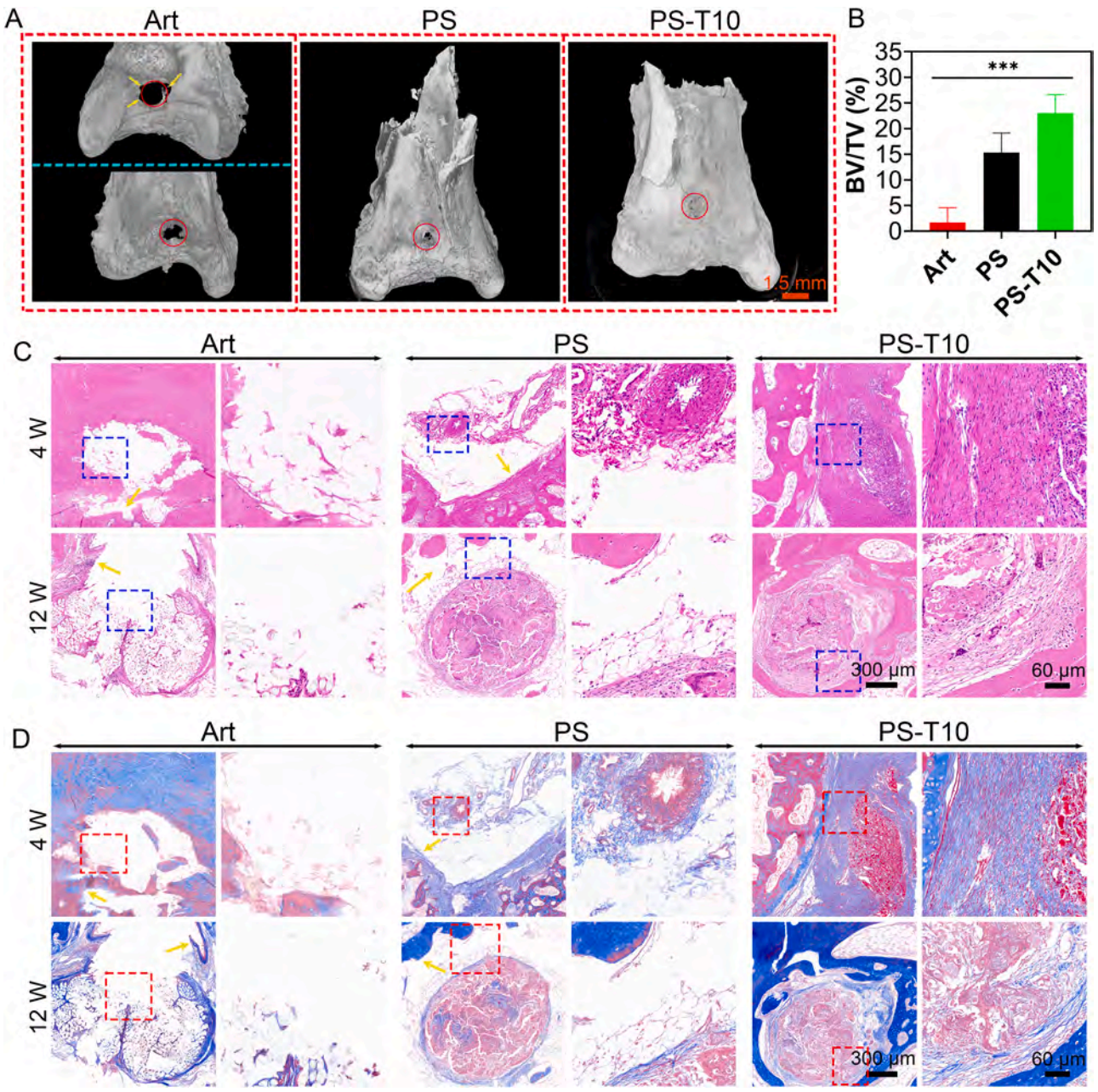

Fig. 9. The ability to osteogenesis *in vivo*. (A) The micro-CT of the calcaneus after 12 weeks, scale bar = 1.5 mm. (B) BV/TV values for Art, PS, PS-T10 sutures. (C) HE staining of Art, PS, PS-T10 sutures in the bone tunnel after 4 and 12 weeks, scale bar = 60 μm, and scale bar = 300 μm. (D) MT staining of Art, PS, PS-T10 sutures in the bone tunnel after 4 and 12 weeks, scale bar = 60 μm, and scale bar = 300 μm. Red circle: the aperture of the original tunnel. Yellow arrows: the gap between the suture and calcaneus. *** $p < 0.001$.

effective mechanical properties, but it is a major source of complications, which can be as high as 30 % [33]. Early studies have shown that tendon graft-bone tunnel healing in both screw-fixed and suture-fixed is the same in terms of pullout strength [34]. Therefore, inexpensive sutures with matching biocompatibility, degradability, and osseointegration for tendon traction and fixation are in demand nowadays compared to expensive, slow degrading, and slow osteoinductive screws. In this study, core-spun nanoyarns containing β-TCP were prepared as surgical sutures. The core layer of the suture consisted of biocompatible SF micron yarns and the shell layer consisted of nanostructured fibers (Fig. 2A), which provided the basis for cell adhesion and proliferation. Due to the suture being assembled from 6 core-spun nanoyarns, it had stronger mechanical properties, which remain stable after 50 mechanical cycles of stretching (Fig. 3B-I). After 8 weeks of degradation, the mechanical properties of the suture fluctuated steadily within a certain range, at which point the suture still maintained its function, whereas the pure SF micron yarn had lost its functionality (Fig. 4). Compared to non-degradable Art, slow degradable suture anchors, and fast degradable pure SF micron yarns, the nanofibers in the shell layer of this suture protected the SF yarns in the core layer, allowing the suture to degrade while ensuring that it did not degrade too quickly. At the same time, Ca^{2+} in the suture could be continuously released for more than 30 days (Fig. 3M), both of which gave the time and conditions for bone formation. It was confirmed in animal experiments. The Art suture was still visible at 4 and 12 weeks, whereas the PS and PS-T10 sutures were visible at 4 weeks but not at 12 weeks (Fig. 8B).

Avinesh et al. [35] used β-TCP grafts for bone-patellar tendon-bone ACL repair, observing a reduction in bone defects. Both animal and

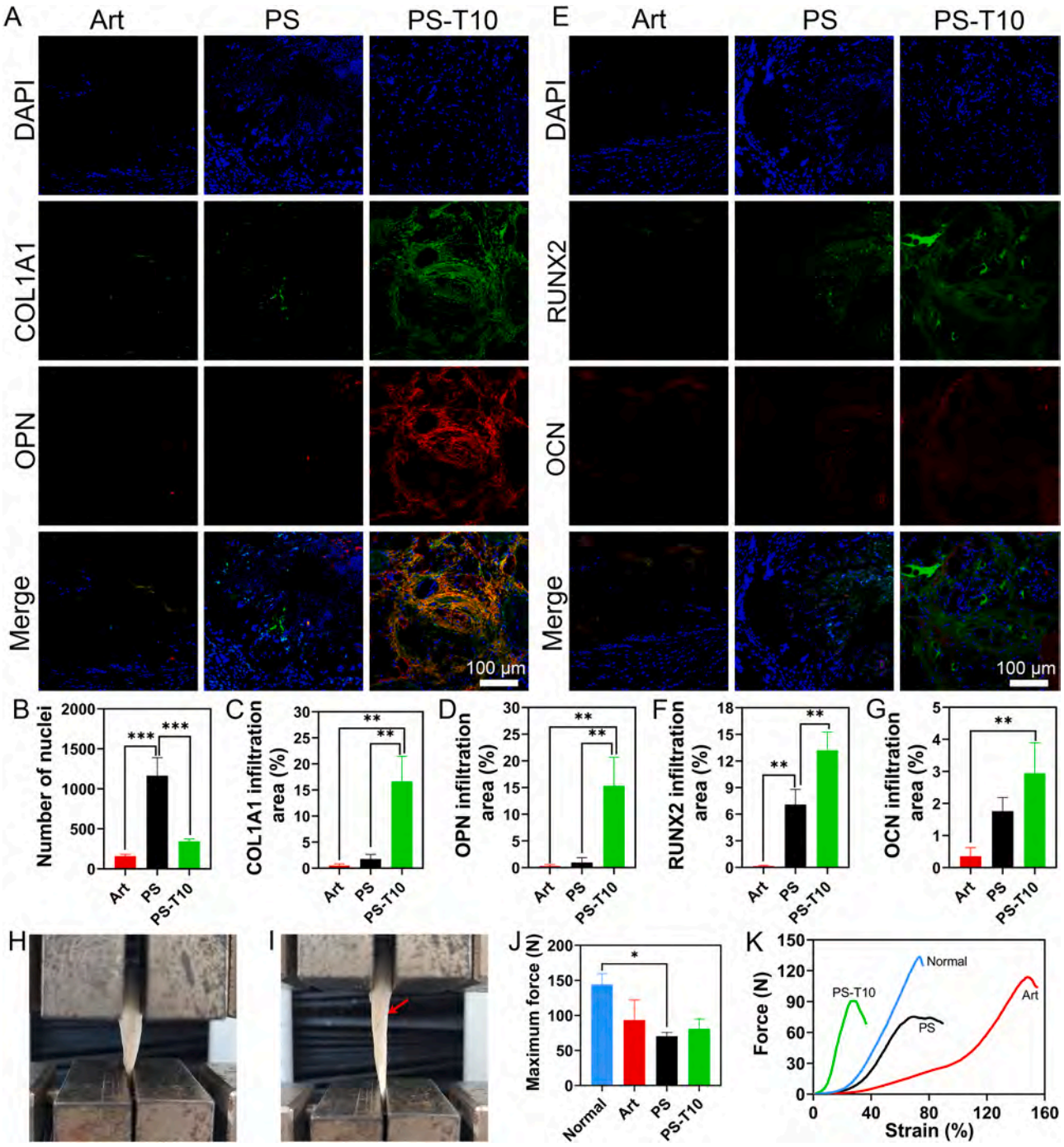

Fig. 10. (A) DAPI/COL1A1/OPN IF staining of Art, PS, PS-T10 sutures in the bone tunnel after 12 weeks, scale bar = 100 μm. The quantification of (B) the number of nuclei, (C) COL1A1 infiltration area, and (D) OPN infiltration area statistics. (E) DAPI/RUNX2/OCN IF staining of Art, PS, PS-T10 sutures in the bone tunnel after 12 weeks, scale bar = 100 μm. The quantification of (F) RUNX2 infiltration area, and (G) OCN infiltration area statistics. (H) The appearance before mechanical stretching, and (I) after mechanical stretching of the Achilles tendon-calcaneus after 12 weeks. (J) The maximum force statistics, and (K) the force-strain curves of normal, Art, PS, PS-T10 groups Achilles tendon-calcaneus after 12 weeks. Red arrow: the location of the Achilles tendon cracked. * $p < 0.05$, ** $p < 0.01$, *** $p < 0.001$.

human cells exhibit normal growth, differentiation, and reproduction on β-TCP, making it a highly promising material for bone repair [36]. In this study, increasing β-TCP content promoted the proliferation of rBMSCs, which grew along the suture, indicating that the suture containing β-TCP was biocompatible (Fig. 6H-J). The PS-T10 group exhibited superior osteogenesis abilities *in vitro* (Fig. 7). These showed that sutures containing β-TCP had the potential to promote new bone formation in bone tunnels and thus increase ruptured tendon stabilization in bone. While numerous studies focus on β-TCP's effects on osteogenesis, there was a paucity of research regarding its impact on tendons. As sutures were essential for weaving the ruptured tendon, the effects of β-TCP-containing sutures on tendons warrant thorough examination. Cellular experiments indicated a proliferation trend of tenocytes on the PS-T10 suture over time, with tenocytes spreading across the suture after 7 days (Fig. 5A and B). More interestingly, the tenocytes in the PS-T10 group showed higher levels of cell number, spreading area, and COL1A1 expression after 10 days than the Art group (Fig. 5C-F). These results demonstrate that β-TCP not only exhibits cytocompatibility with

tenocytes but also promotes COL1A1 secretion, establishing a strong foundation for the integration of the tendon and suture and ensuring stable fixation within the bone.

Ye et al. [37] developed electrospun heparin-loaded nanofiber sutures for the repair of Achilles tendon ruptures, which enhanced the tensile strength of the tendon after surgery. Although there was extensive research on the repair of Achilles tendon rupture, the studies that focused on the Achilles tendon sleeve avulsion model are limited. Consequently, the animal experiments in this study selected the Achilles tendon sleeve avulsion model and the calcaneus-tendon suture method, aiming to achieve stable fixation of the ruptured tendon using β-TCP-containing sutures. This approach represents a significant advancement in treating the less-studied Achilles tendon sleeve avulsion model. In the animal repair model, Art, PS, and PS-T10 sutures effectively wove and fixed the tendon to the calcaneus (Fig. 8B). After 12 weeks, the PS-T10 group demonstrated substantial bone regeneration on micro-CT, and HE and MT staining revealed that the gap between the suture and the bone tunnel was filled with new tissue (Fig. 9). Furthermore, IF staining indicated that PS-T10 sutures significantly induced cells express more COL1A1, OPN, RUNX2, and OCN, signifying increased bone tissue formation and providing greater stability for reconstructive surgery where tendons were anchored to the bone (Fig. 10A-G).

The advent of Art has been a major advance in orthopedic surgery and is commonly used in the clinic for tendon and ligament repair [38, 39]. Art has strong mechanical properties, and the suture-enhanced model can improve graft integrity, ultimate strength, yield strength, and cyclic displacement [40]. However, Art is non-degradable and remains in the bone tunnel for an extended period, impacting the integration of the ruptured tendon and bone. This can lead to slow bone growth within the Art bone tunnel, possibly causing the tunnel to enlarge, posing a risk (Fig. 9). While Art can be left in place after surgery to avoid a second operation, it may develop stress fatigue over time if not removed. Degradable sutures have inferior mechanical properties compared to Art and experience gradual weakening during degradation, an inherent issue with degradable materials. Nonetheless, the tensile strength of degradable synthetic sutures can be enhanced by adjusting material structure and properties. These sutures can also prevent the need for secondary surgery, reduce inflammatory response, and offer similar clinical healing effects as non-absorbable sutures [41]. Liu et al. [42] developed biomimetic, antibacterial, and sensing sutures based on regenerated SF, which could reduce inflammation and bacterial infection, measure the tension of tissues and sutures, and support tissue healing by controlling drug and growth factor release in multiple modes. In this study, the mechanical properties of the surgical suture were ensured by merging 6 core-spun nanoyarns, which could provide stretching and fixation for the ruptured tendon in the initial stage (Fig. 8B). After 12 weeks of mechanical stretching, newly formed bone tissue produced by PS-T10 firmly fixed the tendon to the bone, producing a mechanical effect similar to Art suture (Fig. 10H-K). Over time, new tissue in the bone tunnel replaced the original sutures, which could accelerate tendon fixation to the calcaneus (Fig. 9 and 10A-G). Therefore, PS-T10 suture could not only avoid the risk of bone tunnel enlargement in the Achilles tendon sleeve avulsion model but also improve bone integration, ultimately accelerating tendon rupture repair.

There is an unresolved issue in this study: the nanoyarn sutures created through electrospinning are not as smooth as commercial sutures, resulting in some resistance when suturing tendons. A breakthrough is needed to improve the smoothness of the sutures in future studies.

5. Conclusions

In this study, electrospun sutures containing β-TCP were successfully fabricated with favorable mechanical properties. PS-T10 suture demonstrated the ability to stimulate tenocytes to produce more COL1A1 and up-regulate the expression of COL1A1, OCN, OPN, and RUNX2 in rBMSCs. Animal experiments showed that the suture effectively wove the tendon, pulled and fixed it in the bone tunnel, promoted new bone formation, reduced the gap in the bone tunnel, improved graft fixation stability on the bone, and significantly increased surgical success rates. This study represents a breakthrough in the rarely studied and challenging Achilles tendon sleeve avulsion model.

Data availability

Data will be made available on request.

CRediT authorship contribution statement

Xiao Yu: Writing – review & editing, Writing – original draft, Formal analysis, Data curation. **Genbin Wu:** Writing – original draft, Validation, Formal analysis, Data curation. **Yangfan Ding:** Validation. **Panpan Shang:** Funding acquisition. **Pengfei Cai:** Methodology. **Jie Cui:** Methodology. **Jiahui Song:** Software. **Jinglei Wu:** Supervision. **Mohamed EL-Newehy:** Writing – review & editing. **Meera Moydeen Abdulhameed:** Writing – review & editing. **Xiumei Mo:** Writing – review & editing, Supervision, Funding acquisition. **Yinxian Yu:** Writing – review & editing, Funding acquisition. **Binbin Sun:** Writing – review & editing, Supervision, Investigation, Data curation.

Declaration of competing interest

The authors declare that they have no known competing financial interests or personal relationships that could have appeared to influence the work reported in this paper.

Acknowledgements

This project supported by the Fundamental Research Funds for the Central Universities (CUSF-DH-T-2023063). Science and Technology Commission of Shanghai Municipality, China (20DZ2254900), Sino German Science Foundation Research Exchange Center, China (M-0263), and China Education Association for International Exchange (2022181). This project was also supported by Researchers Supporting Project Number (RSP2025R65), King Saud University, Riyadh, Saudi Arabia. This project was also supported by the grants from the National Natural Science Foundation of China (82302687), and Medicine-Engineering Interdisciplinary Project of Shanghai Jiao Tong University (YG2022QN076). This project was also supported by the Chenguang Program of Shanghai Education Development Foundation and Shanghai Municipal Education Commission (23CGB08).

Supplementary materials

Supplementary material associated with this article can be found, in the online version, at doi:10.1016/j.actbio.2025.03.037.

References

[1] J.Y. Choi, S.S. Lee, T.H. Song, J.S. Suh, A comparison of characteristics and outcomes of operative treatment for Achilles tendon sleeve avulsion in older *versus* younger patients, Arch. Orthop. Trauma Surg. 143 (11) (2023) 6513–6520.
[2] J. Huh, M.E. Easley, J.A. Nunley, Characterization and surgical management of Achilles tendon sleeve avulsions, Foot Ankle Int. 37 (6) (2016) 596–604.
[3] S. Gao, C. Hu, Y. Wang, J. Zhang, K. Tang, Comparison of cortical *versus* cancellous bone fixation in tendon-to-bone healing with a rat trans-calcaneal suture model for Achilles tendon sleeve avulsion, J. Orthop. Surg. Res. 18 (1) (2023) 15.
[4] J. Zhu, B. Marshall, X. Tang, M.A. Linde, F.H. Fu, P. Smolinski, ACL graft with extra-cortical fixation rotates around the femoral tunnel aperture during knee flexion, Knee Surg. Sports Traumatol. Arthrosc. 30 (1) (2022) 116–123.
[5] L. Yue, S.F. DeFroda, K. Sullivan, D. Garcia, B.D. Owens, Mechanisms of bone tunnel enlargement following anterior cruciate ligament reconstruction, JBJS. Rev. 8 (4) (2020) e0120.

[6] A. Borjali, M. Mohseni, M. Chizari, Biomechanical Modeling of a Bone Tunnel Enlargement Post ACL Reconstruction (2020) 281915 bioRxiv 2020.09(03.

[7] D.H. Lee, D.W. Son, Y.R. Seo, I.G. Lee, Comparison of femoral tunnel widening after anterior cruciate ligament reconstruction using cortical button fixation *versus* transfemoral cross-pin fixation: a systematic review and meta-analysis, Knee Surg. Relat. Res. 32 (1) (2020) 11.

[8] T. Zhang, S. Yan, Y. Song, C. Chen, D. Xu, B. Lu, Y. Xu, Exosomes secreted by hypoxia-stimulated bone-marrow mesenchymal stem cells promote grafted tendon-bone tunnel healing in rat anterior cruciate ligament reconstruction model, J. Orthop. Translat. 36 (2022) 152–163.

[9] K.A. Derwin, L.M. Galatz, A. Ratcliffe, S. Thomopoulos, Enthesis repair: challenges and opportunities for effective tendon-to-bone healing, J. Bone Joint Surg. Am. 100 (16) (2018) e109.

[10] H. Lu, C. Chen, S. Xie, Y. Tang, J. Qu, Tendon healing in bone tunnel after Human anterior cruciate ligament reconstruction: a systematic review of histological results, J. Knee Surg. 32 (5) (2019) 454–462.

[11] P. Buttin, B. Goin, T. Cachon, E. Viguier, Repair of tendon disruption using a novel synthetic Fiber implant in dogs and cats: the surgical procedure and three case reports, Vet. Med. Int. 2020 (2020) 4146790.

[12] R. Akoto, M. Albers, M. Balke, B. Bouillon, J. Hoher, ACL reconstruction with quadriceps tendon graft and press-fit fixation *versus* quadruple hamstring graft and interference screw fixation - a matched pair analysis after one year follow up, BMC. Musculoskelet. Disord. 20 (1) (2019) 109.

[13] D.M. Pavao, R.S. Cruz, J.L.R. de Faria, E.B. de Sousa, J.M. Barretto, Modified lemaire lateral tenodesis associated with an intra-articular reconstruction technique with bone-tendon-bone graft using an adjustable fixation mechanism, Arthrosc. Tech. 8 (7) (2019) e733–e740.

[14] T. Matthai, V.M. George, A.S. Rao, A.T. Oommen, R.J. Korula, S. Devasahayam, P. M. Poonnoose, Biomechanical assessment of an alternative method of staple fixation for anchoring the bone patellar tendon bone graft to the tibia, J. Clin. Orthop. Trauma 9 (2) (2018) 157–162.

[15] X. He, Y. Li, H. Miao, J. Xu, M.T.-y. Ong, C. Wang, L. Zheng, J. Wang, L. Huang, H. Zu, Z. Yao, J. Mi, B. Dai, X. Li, P.S.-h. Yung, G. Yuan, L. Qin, High formability Mg-Zn-Gd wire facilitates ACL reconstruction via its swift degradation to accelerate intra-tunnel endochondral ossification, Journal of Magnesium and Alloys 12 (1) (2024) 295–315.

[16] J. Cai, J. Liu, J. Xu, Y. Li, T. Zheng, T. Zhang, K. Han, S. Chen, J. Jiang, S. Wu, J. Zhao, Constructing high-strength nano-micro fibrous woven scaffolds with native-like anisotropic structure and immunoregulatory function for tendon repair and regeneration, Biofabrication 15 (2) (2023) 025002.

[17] X. Yu, G. Shen, J. Yan, W. Guo, Z. Yuan, J. Cui, Y. Shen, P. Cai, Y. Chen, M.T. Ngai, M. El-Newehy, H. El-Hamshary, B. Sun, J. Li, X. Mo, Induction of macrophage polarization by electrospun nano-yarn containing naproxen sodium to promote tendon repair, Appl. Mater. Today 36 (2024) 102070.

[18] X. Yu, Y. Shen, J. Cui, Y. Ding, Y. Morsi, B. Sun, X. Mo, H. Gu, The potential application of electrical stimulation in tendon repair: a review, Med-X 3 (2025) 7.

[19] Y. Chen, M. Shafiq, M. Liu, Y. Morsi, X. Mo, Advanced fabrication for electrospun three-dimensional nanofiber aerogels and scaffolds, Bioact. Mater. 5 (4) (2020) 963–979.

[20] J. Cai, J. Wang, K. Ye, D. Li, C. Ai, D. Sheng, W. Jin, X. Liu, Y. Zhi, J. Jiang, J. Chen, X. Mo, S. Chen, Dual-layer aligned-random nanofibrous scaffolds for improving gradient microstructure of tendon-to-bone healing in a rabbit extra-articular model, Int. J. Nanomedicine 13 (2018) 3481–3492.

[21] Y. Chen, X. Dong, M. Shafiq, G. Myles, N. Radacsi, X. Mo, Recent advancements on three-dimensional electrospun nanofiber scaffolds for tissue engineering, Adv. Fiber. Mater. 4 (5) (2022) 959–986.

[22] Y. Lin, L. Zhang, N.Q. Liu, Q. Yao, B. Van Handel, Y. Xu, C. Wang, D. Evseenko, L. Wang, *In vitro* behavior of tendon stem/progenitor cells on bioactive electrospun nanofiber membranes for tendon-bone tissue engineering applications, Int. J. Nanomedicine 14 (2019) 5831–5848.

[23] P. Chen, L. Li, L. Dong, S. Wang, Z. Huang, Y. Qian, C. Wang, W. Liu, L. Yang, Gradient biomineralized silk fibroin nanofibrous scaffold with osteochondral inductivity for integration of tendon to bone, ACS. Biomater. Sci. Eng. 7 (3) (2021) 841–851.

[24] H. Goodarzi, S. Hashemi-Najafabadi, N. Baheiraei, F. Bagheri, Preparation and characterization of nanocomposite scaffolds (Collagen/beta-TCP/SrO) for bone tissue engineering, Tissue Eng. Regen. Med. 16 (3) (2019) 237–251.

[25] R. Urruela-Barrios, E. Ramirez-Cedillo, A. Diaz de Leon, A.J. Alvarez, W. Ortega-Lara, Alginate/gelatin hydrogels reinforced with TiO(2) and beta-TCP fabricated by microextrusion-based printing for tissue regeneration, Polymers. (Basel) 11 (3) (2019) 457.

[26] X. Liu, X. He, D. Jin, S. Wu, H. Wang, M. Yin, A. Aldalbahi, M. El-Newehy, X. Mo, J. Wu, A biodegradable multifunctional nanofibrous membrane for periodontal tissue regeneration, Acta Biomater. 108 (2020) 207–222.

[27] S. Jiang, X. Zhao, S. Chen, G. Pan, J. Song, N. He, F. Li, W. Cui, C. Fan, Down-regulating ERK1/2 and SMAD2/3 phosphorylation by physical barrier of celecoxib-loaded electrospun fibrous membranes prevents tendon adhesions, Biomaterials 35 (37) (2014) 9920–9929.

[28] D.A. Brennan, A.A. Conte, G. Kanski, S. Turkula, X. Hu, M.T. Kleiner, V. Beachley, Mechanical considerations for electrospun nanofibers in tendon and ligament repair, Adv. Healthc. Mater. 7 (12) (2018) 1701277.

[29] S. Kurihara, S. Yanagisawa, T. Takahashi, K. Hagiwara, K. Hatayama, R. Takase, M. Kimura, H. Chikuda, Increased bone plug depth from the joint increases tunnel enlargement in anterior cruciate ligament reconstruction using bone–Patellar tendon–Bone autograft with suspensory femoral fixation, Arthrosc. Sports Med. Rehabil. 5 (4) (2023) 100755.

[30] K. Boksh, A. Haque, A. Sharma, P. Divall, H. Singh, Use of suture tapes versus conventional sutures for arthroscopic rotator cuff repairs: a systematic review and meta-analysis, Am. J. Sports Med. 50 (1) (2021) 264–272.

[31] R. Gupta, S. Singh, A. Kapoor, A. soni, R. Kaur, N. Kaur, Graft tunnel integration occurs early in the tibial tunnel compared with the femoral tunnel after anterior cruciate ligament reconstruction with preserved insertion hamstring tendon graft, Knee Surg. Relat. Res. 33 (1) (2021) 1–7.

[32] M. Sgroi, T. Friesz, M. Schocke, H. Reichel, T. Kappe, Biocomposite suture anchors remain visible two years after rotator cuff repair, Clinical Orthopaedics & Related Research 477 (6) (2019) 1469–1478.

[33] P. Boileau, P. Gendre, D.J. Saliken, C.-É. Thélu, C. Trojani, Tensioning device increases coracoid bone block healing rates in arthroscopic Latarjet procedure with suture-button fixation, J. Shoulder. Elbow. Surg. 31 (7) (2022) 1451–1462.

[34] H. Kawakami, K. Shino, M. Hamada, K. Nakata, S. Nakagawa, N. Nakamura, Y. Toritsuka, H. Yoshikawa, T. Ochi, Graft healing in a bone tunnel: bone-attached graft with screw fixation *versus* bone-free graft with extra-articular suture fixation, Knee Surgery, Sports Traumatology, Arthroscopy 12 (5) (2004) 384–390.

[35] A. Agarwalla, R. Puzzitiello, G.H. Garcia, B. Forsythe, Application of a beta-tricalcium phosphate graft to minimize bony defect in bone–Patella tendon–Bone anterior cruciate ligament reconstruction, Arthrosc. Tech. 7 (7) (2018) e725–e729.

[36] W. Wang, P. Liu, B. Zhang, X. Gui, X. Pei, P. Song, X. Yu, Z. Zhang, C. Zhou, Fused deposition modeling printed PLA/nano β-TCP composite bone tissue engineering scaffolds for promoting osteogenic induction function, International Journal of Nanomedicine 18 (2023) 5815–5830.

[37] Y. Ye, Y. Zhou, Z. Jing, Y. Xu, D. Yin, Electrospun heparin-loaded nano-fiber sutures for the amelioration of achilles tendon rupture regeneration: *in vivo* evaluation, Journal of Materials Chemistry B 9 (20) (2021) 4154–4168.

[38] C. Lavender, B. Johnson, A. Kopiec, Augmentation of anterior cruciate ligament reconstruction with bone marrow concentrate and a suture tape, Arthrosc. Tech. 7 (12) (2018) e1289–e1293.

[39] D.M. Benson, G.P. Hopper, W.T. Wilson, G.M. Mackay, Anterior cruciate ligament reconstruction using bone–Patellar tendon–Bone autograft with suture tape augmentation, Arthrosc. Tech. 10 (2) (2021) e249–e255.

[40] V.J. Lai, A.W. Reynolds, M. Kindya, J. Konicek, S. Akhavan, The use of suture augmentation for graft protection in ACL reconstruction: a biomechanical study in porcine knees, Arthrosc. Sports Med. Rehabil. 3 (1) (2021) e57–e63.

[41] Y. Li, Q. Meng, S. Chen, P. Ling, M.A. Kuss, B. Duan, S. Wu, Advances, challenges, and prospects for surgical suture materials, Acta Biomater. 168 (2023) 78–112.

[42] M. Liu, Y. Zhang, K. Liu, G. Zhang, Y. Mao, L. Chen, Y. Peng, T.H. Tao, Biomimicking antibacterial opto-electro sensing sutures made of regenerated silk proteins, Advanced Materials 33 (1) (2021) 2004733.